


 Cite this: *RSC Adv.*, 2021, **11**, 17828

Theoretical insights into the electroreduction mechanism of N_2 to NH_3 from an improved Au(111)/ H_2O interface model†

Lihui Ou, * Junling Jin* and Yuandao Chen

An improved H coverage-dependent Au(111)/ H_2O electrochemical interface model is proposed in this paper, which is firstly used to study electroreduction mechanisms of N_2 into NH_3 at the thermodynamical equilibrium potential in cooperation with electronic structure analysis. The results show that the associative mechanism is more favorable on Au(111) and therein alternating and distal pathways may be able to parallelly occur in gas phase and the present simulated electrochemical interface. The initial N_2 reduction into the N_2H intermediate is the rate determining step, which may be able to be regarded as the origin of the observed experimentally high overpotential during N_2 electroreduction. The presence of an electrochemical environment can significantly change the N_2 reduction pathway and decrease the barrier of the rate determining step, which can be ascribed to the significant electron accumulation and interaction between N_2 molecules and H_2O clusters. The theoretical results display excellent consistency with the available experimental data, confirming the rationality of the present proposed electrochemical model. The comparison of the barrier between the hydrogen evolution reaction and rate determining step well explains why the activity of Au electrodes is usually unsatisfactory. Accordingly, a single descriptor can be proposed, in which an ideal electrocatalyst should be able to reduce the barrier for initial N_2 electroreduction into N_2H . In this way, N_2 electroreduction pathways can be facilitated and the yield of NH_3 can be enhanced. We believe that the present study can represent progress to study N_2 electroreduction mechanisms from an improved electrochemical model.

 Received 12th March 2021
 Accepted 7th May 2021

 DOI: 10.1039/d1ra01978c
rsc.li/rsc-advances

1. Introduction

NH_3 as a promising carbon-free alternative energy carrier can be employed in fertilizers, production of important chemicals, NH_3 fuel cells and indirectly hydrogen fuel cells.^{1–3} At present, NH_3 is synthesized primarily by reaction of N_2 with H_2 on an Fe/Ru-based catalyst through the industrial Haber–Bosch (HB) process under harsh conditions such as high temperatures and pressures,^{4,5} which is an energy intensive chemical process and consumes *ca.* 2% of annual global energy because of the stability and chemical inertness of N_2 molecule.^{6–8} By contrast, the electrochemical reduction of N_2 into NH_3 with proton and electron transfer in an aqueous environment is more energy efficient and attracts extensive interest in recent years since it can be operated at ambient conditions and powered by

renewable electricity.^{9–14} Unfortunately, the required large overpotential and competing hydrogen evolution reaction lead to low faradaic efficiency and poor selectivity for N_2 electroreduction into NH_3 on most electrocatalysts, thus impeding its practical applications.^{15–18} The poor activity of the cathode electrocatalyst may put a major limitation on production of NH_3 product in significant yields at ambient conditions. To achieve the rational design of more selective and active electrocatalysts, the system understanding on electroreduction mechanism of N_2 into NH_3 is extremely urgent and essential.

Although tremendous efforts in recent years, N_2 electroreduction mechanism remains elusive. The present most studies on N_2 electroreduction reaction primarily focus on the synthesis of electrocatalysts including metals such as Pt, Ru, Fe, Au, Pd, Rh, Fe, Ni, Mo and Bi,^{19–30} alloys such as Pt–Ru,³¹ metal nitrides and sulfides,^{32,33} and carbon-based materials.^{34–38} However, these reported electrocatalysts suffer from low NH_3 faradaic efficiency and N_2 electroreduction reaction is still plagued. Based on these previous studies, the development of more active and selective electrocatalysts is highly desired but remains challenging. Study of N_2 electroreduction reaction mechanism will help design electrocatalysts with high activity and selectivity. In the most recent reviews from Shao *et al.* and

Hunan Province Cooperative Innovation Center for the Construction & Development of Dongting Lake Ecologic Economic Zone, Hunan Provincial Key Laboratory of Water Treatment Functional Materials, Hunan Province Engineering Research Center of Electropating Wastewater Reuse Technology, College of Chemistry and Materials Engineering, Hunan University of Arts and Science, Changde, 415000, China.
 E-mail: lihuiou@huas.edu.cn; jinjl174@nenu.edu.cn

† Electronic supplementary information (ESI) available. See DOI: 10.1039/d1ra01978c



Zhang *et al.*,^{39,40} N_2 electroreduction mechanisms and reaction intermediates that obtained in experiments by various spectroscopy techniques are summarized. Currently, it is generally accepted that there are two main reaction mechanisms for N_2 electroreduction into NH_3 , namely, dissociative pathways and associative pathways. $\text{N}\equiv\text{N}$ bond in N_2 molecule is broken to form N atoms on electrocatalyst surface before hydrogenation in dissociative mechanism, whereas the hydrogenation of N_2 molecule occurs before $\text{N}\equiv\text{N}$ bond is broken in associative mechanism. It is currently believed that the dissociative mechanism is dominant in the HB process of N_2 reduction into NH_3 .^{15,41} An associative distal or alternating mechanism may be followed during N_2 electroreduction into NH_3 through experimental identification of some intermediates. For example, using surface-enhanced infrared absorption spectroscopy, Shao *et al.*, studied for the first time N_2 electrochemical reduction reaction mechanism on Au thin film, in which the adsorbed N_2H_y ($1 \leq y \leq 4$) species was detected at potentials below 0 V (vs. RHE),⁴² thus indicating that N_2 electroreduction may follow the associative alternating and distal mechanisms on Au surface. Combing surface-enhanced infrared absorption spectroscopy with electrochemical measurements, the adsorbed N_2H_x ($0 \leq x \leq 2$) species was detected at potentials below 0.2 V (vs. RHE) on Ru thin film in the subsequent study from Shao *et al.*, and notably increased coverage of N_2H_x was observed as the potential decreasing from 0.2 to -0.4 V, thus the associative distal mechanism may be able be concluded.²⁰ By performing isotope-labelled experiments, Yin *et al.*, found only a trace amount of N_2H_4 intermediate during N_2 electroreduction on bismuth surface, suggesting that associative distal mechanism may be more favorable.³⁰ Despite of understanding of N_2 electroreduction reaction mechanism is of importance for rationally designing more efficient electrocatalysts, the experimental studies are very rare at present in this area since low selectivity makes experimental determination of mechanism rather difficult.

Because of the experimental limitations to identify intermediates and complexity of N_2 electroreduction process involving 6 elementary reaction steps, theoretical calculations have become a powerful tool for studying electrocatalytic reactions by employing density functional theory (DFT).^{43,44} DFT calculations can give mechanistic information that is not accessible based on experiments alone and identify favored reaction intermediates. Theoretical work by Skúlason *et al.* and Montoya *et al.* thermodynamically indicated that the associative distal mechanism would be more favorable since more positive reaction free energies are expected for the associative alternating mechanism by combining DFT calculations with the computational hydrogen electrode model.^{15,45} Their findings had shown that the potential limiting step is N_2 reductive protonation to the adsorbed N_2H species on the transition metal surface with relatively weak N adsorption such as Pt, Pd, Ag, Au, Ni, Co and Ru during N_2 electroreduction into NH_3 , whereas the potential limiting step is determined by the protonation of the adsorbed NH into NH_2 species for more reactive transition metals, such as Mo. On the basis of DFT-based computational hydrogen electrode model, the electrocatalytic activity of various binary transition metals are systematically examined in recent theoretical work from Zhao

et al.,⁴⁶ and the binary FeRh catalyst was thought to have the optimal catalytic performance due to its lowest limiting potential and best suppressing effect on hydrogen evolution reaction during N_2 electroreduction reaction. Furthermore, their study indicated that N_2 reduction reaction prefers to proceed through associative distal mechanisms than alternating pathways on the FeRh catalyst. These above theoretical studies assumed that activation barriers of reaction pathways is related with reaction free energies on different transition metal surfaces and only considered various elementary step thermodynamics, whereas the potential-dependent kinetic barriers that predicting catalytic activity were not further calculated. Most recently, Janik *et al.* calculated explicitly the potential-dependent activation barriers for elementary electroreduction reactions included in associative distal and alternating pathways during N_2 electroreduction using their previously developed method,^{47–49} and concluded that the alternating mechanism by direct surface hydrogenation may be more favorable on late transition metals due to smaller barriers at 0 V (vs. RHE),^{50,51} in which N_2 electroreduction into N_2H species is rate determining step of overall reaction. However, despite various theoretical efforts, N_2 electroreduction mechanisms are still not systematically understood and mechanistic inconsistencies remain exist. Furthermore, the key factor such as solvent effect was not included in previous theoretical studies on N_2 electroreduction mechanisms. Thus, the modeling of electrocatalytic reaction systems occurred at the complex electrode/aqueous interfaces remains a subject of ongoing discussion.

In the present paper, Au electrocatalyst is selected due to its excellent durability, relatively high faradaic efficiency and low hydrogen evolution reaction activity in N_2 electroreduction. Furthermore, electrocatalytic N_2 reduction reaction on the Au surface is indeed possible under ambient conditions.^{25,52} Our previous validated explicit solvation model with two relaxed H_2O bilayer structure is employed to simulate solvent effect,^{53–55} which allows us to better model the interactions among adsorbates, surface and solvents and determine the kinetic barriers for various elementary reaction steps. Thus, an improve H coverage-dependent Au(111)/ H_2O electrochemical interface model is proposed, by which the electroreduction mechanisms of N_2 into NH_3 can be identified. Simultaneously, solvation effect on N_2 reduction mechanisms is also considered in this work. Our present used model is differentiated from previous theoretical work on N_2 electroreduction into NH_3 . The available experimental results on Au electrodes will be used to examine whether the currently employed computational model is enough accurate by comparing with our present theoretical study.

2. H coverage-dependent Au(111)/ H_2O interface model

2.1 Determination method of equilibrium potentials

Surface and solvation model, and computational parameters included in computational details have been represented in detail in ESI (see Fig. S1).† It is known that the hydrogen evolution reaction and proton-coupled electron transfer usually occur during N_2 electroreduction on the Au electrodes, thereby



the surface adsorbed H atoms as the intermediate may be involved.^{24,25,53} Moreover, the difference of electrostatic potential in electric double layer can be controlled and adjusted by changing number of the surface adsorbed H atoms.⁵⁶⁻⁵⁸ Thus, the H coverage-dependent equilibrium potentials can be determined and potential-dependent N₂ electroreduction mechanisms can be speculated. The surface adsorbed H atom can be formed during N₂ electroreduction by following eqn (1):



At different H coverage conditions, the Gibbs free energy of eqn (1), $\Delta G(\theta)$ can be calculated by eqn (2) on the basis of the methodology proposed by Nørskov *et al.*, Chen *et al.* and Strasser *et al.* for oxygen reduction, hydrogen evolution and CO₂ electrochemical reduction reactions,^{56,59-63} in which $\Delta E(\theta)$, $\Delta S(\theta)$, ΔZPE and $k_{\text{B}}T \ln(\theta/1 - \theta)$ represent the differential adsorption energy of surface adsorbed H atoms, entropy change, zero-point energy change and the contributions of configuration entropy to $\Delta G(\theta)$, respectively. Herein, coverage $\theta = n/N$, in which n is the number of surface adsorbed H atoms and N is the total number of surface Au atoms. Thus, the H coverage-dependent equilibrium potential U (vs. RHE) can be determined at Au(111)/H₂O interface when the Gibbs free energy, $\Delta G(\theta)$ is equal with zero.

$$\Delta G(\theta) = \Delta E(\theta) + eU - T\Delta S(\theta) + \Delta ZPE + k_{\text{B}}T \ln(\theta/1 - \theta) \quad (2)$$

According to eqn (3), the differential adsorption energy of surface adsorbed H atoms, $\Delta E(\theta)$ can be calculated, where $E(\theta)_{M_{\text{H}_n}}$ is the total energy of the Au surface with different coverage of adsorbed H atoms.

$$\begin{aligned} \Delta E(\theta) &= \partial E(\theta)_{M_{\text{H}_n}} / \partial n - \frac{1}{2}E_{\text{H}_2} \\ &= \partial E(\theta)_{M_{\text{H}_n}} / N \partial \theta - \frac{1}{2}E_{\text{H}_2} \end{aligned} \quad (3)$$

The contributions from ZPE and entropy changes together to $\Delta G(\theta)$ are estimated to be *ca.* 0.24 eV at standard temperature

(298 K) based on the available data from previous literature.⁶⁴ Therefore, combining eqn (2) with eqn (3), the eqn (4) can be obtained. The values of $E(\theta)_{M_{\text{H}_n}}$ and E_{H_2} is directly available *via* DFT calculations. A series of values of $E(\theta)_{M_{\text{H}_n}}$ can be calculated by changing the coverage of surface adsorbed H atoms on Au(111). At the different coverages, the values of $\Delta E(\theta)$ can be obtained by differentiating the plots of $\partial E(\theta)_{M_{\text{H}_n}}/N$ against θ on the basis of eqn (3).

$$\begin{aligned} \Delta G(\theta) &= \left[\partial E(\theta)_{M_{\text{H}_n}} / N \partial \theta - \left(\frac{1}{2}E_{\text{H}_2} - eU \right) \right] + 0.24 \\ &+ k_{\text{B}}T \ln(\theta/1 - \theta) \end{aligned} \quad (4)$$

2.2 Relationship between H coverage and equilibrium potentials

In the present study, we consider various possible surface adsorption configurations of H atoms and coverage dependence. It is observed that H atoms prefer to adsorb at 3-fold face-centered cubic hollow (fcc) sites on Au(111) so that they can stay away from each other in order to minimize the repulsive reactions when H coverage (θ_{H}) is below and equal with 1 monolayer (ML) (see Fig. S2†). The coverages of H atoms above 1 ML are not further analyzed on Au(111) because of the observed spontaneous formations of hydrate proton by adsorbed H atoms with adjacent H₂O molecules caused by strong repulsive interactions among adsorbed H atoms. Fig. 1(a) exhibits a reasonable polynomial relationship between the differential adsorption energy of surface adsorbed H atoms, $\Delta E(\theta)$ and θ_{H} , indicating that the Langmuir adsorption isotherms may be followed on Au(111). Thereby, $\Delta E(\theta)$ can be calculated at any θ_{H} through polynomial fitting of $\Delta E(\theta) \sim \theta_{\text{H}}$ data. We can calculated the equilibrium potentials (U) based on the eqn (4) at any θ_{H} and then the polynomial relationships between θ_{H} and U can be obtained on Au(111). It is found that the more negative equilibrium potentials can be obtained with the increasing H coverage, as shown in Fig. 1(b). In fact, the previous theoretical study from Skúlason *et al.* also showed that most surfaces will be fully covered with the adsorbed H atoms at more negative

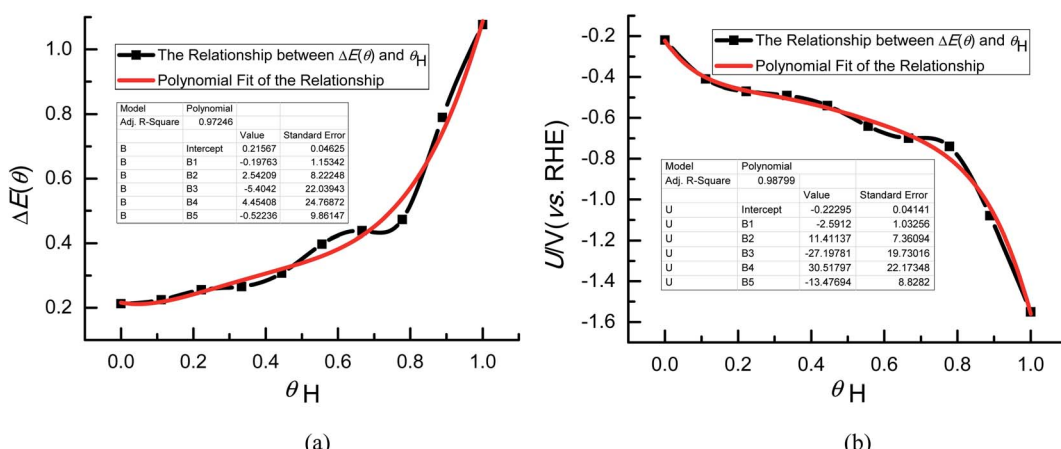


Fig. 1 (a) The relationship between the differential adsorption energy of H atoms and H coverage (θ_{H}), $\Delta E(\theta)$; (b) the relationship between the calculated equilibrium potentials (U) and H coverage (θ_{H}).



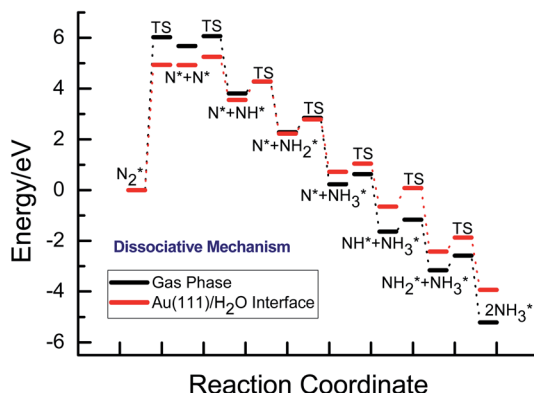


Fig. 2 Overall energy pathway diagram of N_2 reduction and electro-reduction into NH_3 via dissociative mechanism on $\text{Au}(111)$ in gas phase and the present simulated $\text{Au}(111)/\text{H}_2\text{O}$ electrochemical interface.

electrode potentials,⁵⁶ confirming the reasonability of our present proposed H coverage-dependent $\text{Au}(111)/\text{H}_2\text{O}$ electrochemical interface model to some degree. The equilibrium potential is calculated as *ca.* -0.22 V (vs. RHE) when θ_{H} is equal with zero based on the polynomial relationship between θ_{H} and U , which is the closest to the thermodynamical value of *ca.* -0.06 V (vs. RHE) for N_2 electroreduction under ambient conditions,²⁰ thus being regarded as the thermodynamical equilibrium potential. Our present study will focus on the electroreduction mechanisms of N_2 into NH_3 at the thermodynamical required equilibrium potential with the aim of applying the present proposed H coverage-dependent $\text{Au}(111)/\text{H}_2\text{O}$ interface model. The mechanistic understanding on N_2 electroreduction can provide scientific guideline for rational design of efficient electrocatalysts. The potential-dependent N_2 electroreduction mechanisms will be further studied in our future work.

3. Results and discussion

3.1 N_2 reduction mechanism on $\text{Au}(111)$ in gas phase

For comparison and consideration of solvation effect on N_2 reduction mechanisms, we firstly present calculated results of N_2 reduction to NH_3 via dissociative and associative

mechanisms on $\text{Au}(111)$ in gas phase. In dissociative mechanism, N_2 is initially dissociated to form the adsorbed N atoms on $\text{Au}(111)$ with an extremely high activation barrier of *ca.* 6.02 eV, as can be seen in Fig. 2. Subsequently, the adsorbed N atoms are further reduced to form NH_3 molecules *via* serial surface hydrogenation steps with corresponding barriers of *ca.* 0.40 , 0.47 and 0.57 eV, respectively. By comprehensively scrutinizing the overall energy pathway diagram of N_2 reduction into NH_3 in gas phase, N_2 dissociation pathway is rate determining step of overall reaction in dissociative mechanism on $\text{Au}(111)$.

Fig. 3 shows the overall energy pathway diagram of N_2 reduction into NH_3 *via* associative alternating and distal mechanisms in gas phase. In these both mechanisms, the activation barrier is calculated as *ca.* 2.10 eV for the first hydrogenation step of N_2 molecule into the adsorbed N_2H species. Beginning with the further reduction of N_2H , there may be two possibilities to occur. One is N_2H hydrogenation to form the surface adsorbed NHNH species, which is defined alternating pathways; another is N_2H hydrogenation to form the surface adsorbed NNH_2 species, being defined as distal pathways. The required barrier for the formation of NHNH species is *ca.* 0.17 eV in alternating pathways. NHNH species can further be reduced to form the adsorbed NNH_2 species with an activation barrier of *ca.* 0.26 eV. Two possibilities are considered for NNH_2 subsequent further reduction, the adsorbed NH_2NH_2 and NHNH_3 species may be formed *via* surface hydrogenation. The corresponding barrier is 0.31 and 0.21 eV, respectively, which is extremely low and surmountable at room temperature, indicating that NHNH_2 further reduction into NH_2NH_2 and NHNH_3 species may be parallel pathways in alternating pathways. NH_2NH_2 further reduction to form the first NH_3 molecule may be able to be separated into two elementary reaction steps, namely, NH_2NH_2 species surface hydrogenation into the adsorbed NH_2NH_3 species, and subsequent formation of the adsorbed NH_2 species and NH_3 product *via* N–N bond cleavage. The calculated barrier is *ca.* 0.37 and 1.66 eV, respectively, as shown in Fig. 3(a). Surface hydrogenation of NH_2 intermediate can finally leads to production of the second NH_3 molecule.

In distal pathways, surface hydrogenation of NNH_2 intermediate is possible to form the adsorbed NNH_3 and NHNH_2 species. However, the significant higher barrier for formation of

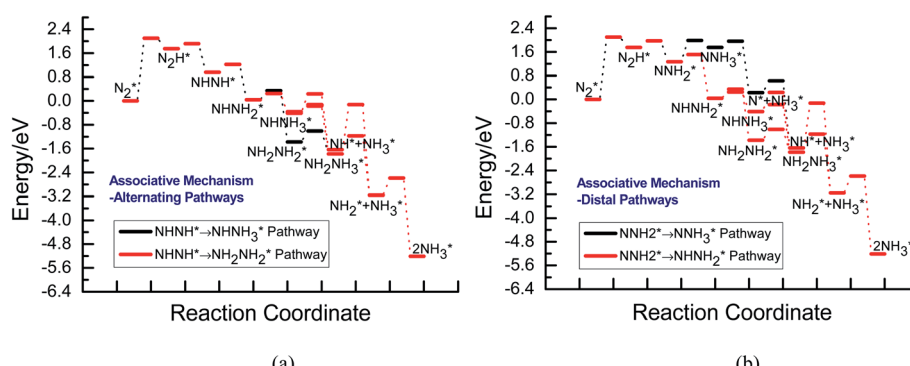


Fig. 3 Overall energy pathway diagram of N_2 reduction into NH_3 *via* associative mechanism on $\text{Au}(111)$ in gas phase: (a) alternating pathways; (b) distal pathways.



Table 1 Activation barriers (ΔE_{act} , eV) and reaction energies (ΔE_{reac} , eV) for the possible elementary reaction steps involved in N_2 reduction pathways on Au(111) in gas phase

Elementary reaction steps ^a	ΔE_{act} , eV	ΔE_{reac} , eV
$\text{N}_2 + * \rightarrow \text{N}^* + \text{N}^*$	6.02	5.67
$\text{N}^* + \text{H}^* \rightarrow \text{NH}^*$	0.40	-1.87
$\text{NH}^* + \text{H}^* \rightarrow \text{NH}_2^*$	0.47	-1.52
$\text{NH}_2^* + \text{H}^* \rightarrow \text{NH}_3^*$	0.57	-2.05
$\text{N}_2 + \text{H}^* \rightarrow \text{N}_2\text{H}^*$	2.10	1.75
$\text{N}_2\text{H}^* + \text{H}^* \rightarrow \text{NHNH}^*$	0.17	-0.79
$\text{N}_2\text{H}^* + \text{H}^* \rightarrow \text{NNH}_2^*$	0.22	-0.48
$\text{NHNH}^* + \text{H}^* \rightarrow \text{NHNH}_2^*$	0.26	-0.92
$\text{NNH}_2^* + \text{H}^* \rightarrow \text{NNH}_3^*$	0.24	-1.23
$\text{NNH}_2^* + \text{H}^* \rightarrow \text{NNH}_2^*$	0.72	0.48
$\text{NNH}_2^* + \text{H}^* \rightarrow \text{NNH}_2\text{NH}_2^*$	0.31	-1.42
$\text{NNH}_2\text{NH}_2^* + \text{H}^* \rightarrow \text{NNH}_3^*$	0.21	-0.45
$\text{NNH}_3^* \rightarrow \text{N}^* + \text{NH}_3^*$	0.21	-1.52
$\text{NH}_2\text{NH}_2^* + \text{H}^* \rightarrow \text{NH}_2\text{NH}_3^*$	0.37	-0.40
$\text{NNH}_3^* + \text{H}^* \rightarrow \text{NH}_2\text{NH}_3^*$	0.24	-1.37
$\text{NNH}_3^* \rightarrow \text{NH}^* + \text{NH}_3^*$	0.65	-1.23
$\text{NH}_2\text{NH}_3^* \rightarrow \text{NH}_2^* + \text{NH}_3^*$	1.66	-1.38

^a The asterisk (*) indicates that the species is adsorbed on the Au(111) surface.

NNH₃ than NHNH₂ is observed (0.72 eV vs. 0.24 eV), indicating that the NNH₃ formation is kinetically inhibited, as shown in Fig. 3(b). Starting with NHNH₂ further reduction, the first NH₃ molecule may be produced *via* two elementary reaction steps involving hydrogenation into the adsorbed NNH₃ species and

its subsequent N–N bond scission with the formations of the adsorbed NH species and NH₃ product, and the corresponding barrier is calculated as *ca.* 0.21 and 0.65 eV. The adsorbed NH₂NH₂ intermediate is also possible to be formed through NHNH₂ surface hydrogenation with the surmountable barrier of *ca.* 0.31 eV at room temperature in distal pathways. As above elaborated, NH₂NH₂ species can further be reduced into the adsorbed NH₂ species and the first NH₃ molecule *via* surface hydrogenation and N–N bond scission. The adsorbed NH and NH₂ intermediates can finally lead to the second NH₃ molecule *via* surface hydrogenation in distal pathways. However, we note that the extremely high barrier is required for N–N bond cleavage in NH₂NH₃ species to form NH₃ product (*ca.* 1.66 eV) in associative alternating and distal mechanisms, thereby it can be concluded that NH₂NH₃ species is only a spectator during N₂ reduction in gas phase due to its easy formation *via* NHNH₃ and NH₂NH₂ hydrogenation. The corresponding energetics of for the possible elementary reaction steps involved in N₂ reduction pathways on Au(111) in gas phase are summarized in Table 1.

By scrutinizing the overall energy pathway diagram of associative alternating and distal mechanisms (see Fig. 3), N₂ hydrogenation into N₂H species is rate determining step with the barrier of *ca.* 2.10 eV, suggesting that both alternating and distal pathways may be parallel and operable on Au(111) in gas phase. It is found that the barrier of rate determining step for the associative mechanism is notably lower than that of dissociative mechanism by comparing the barriers between these both mechanisms (*ca.* 2.10 eV vs. 6.02 eV), suggesting that the associative mechanism including the adsorbed NHNH, NNH₂, NH₂NH₂, NHNH₃ and NH₂NH₃ intermediates is more favorable.

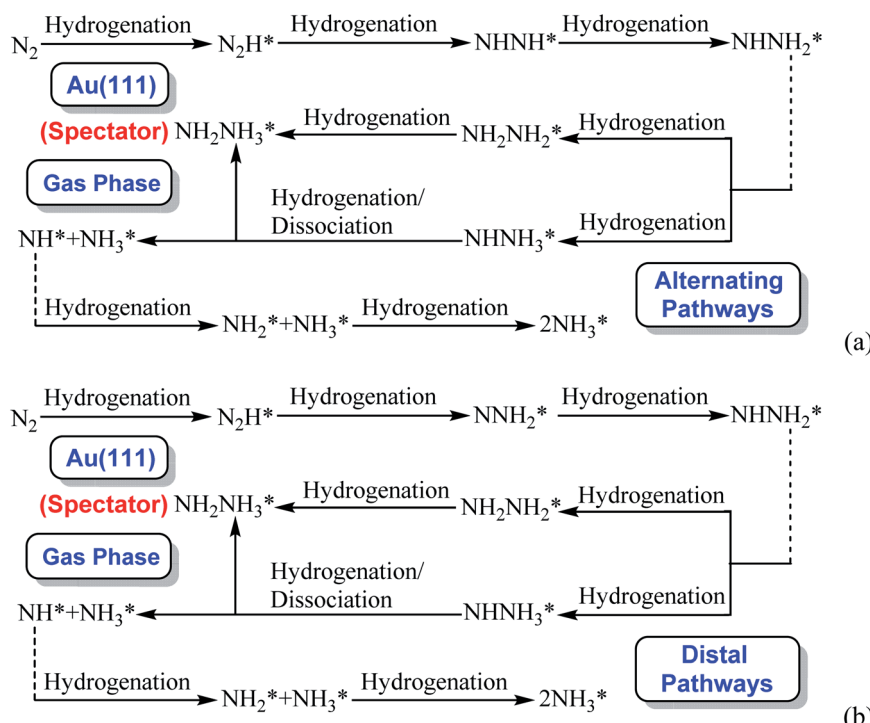


Fig. 4 The optimal associative mechanisms on Au(111) in gas phase: (a) alternating pathways *via* NHNH species; (b) distal pathways *via* NNH₂ species (* represents surface adsorption).



The optimal associative mechanisms including alternating and distal pathways on Au(111) in gas phase are summarized in Fig. 4. Images of reactants, products and transition states for N_2 reduction into NH_3 via the optimal associative mechanisms are included in ESI, as shown in Fig. S3–S13.† However, we also note that the required barrier for initial N_2 hydrogenation is extremely high, which may be able to be ascribed to weakly bonded N_2 molecule on Au(111) with the adsorption energy of *ca.* -0.03 eV. Furthermore, $\text{N}\equiv\text{N}$ bond length of N_2 on Au(111) is almost identical with that of isolated N_2 molecule, *ca.* 1.11 Å.

3.2 N_2 electroreduction mechanism at Au(111)/ H_2O interface

Our present proposed H coverage-dependent Au(111)/ H_2O electrochemical interface model is utilized to simulate N_2 electroreduction pathways, including dissociative and associative mechanisms. The present calculated thermodynamically required equilibrium potential of *ca.* -0.22 V (vs. RHE) when θ_{H} is equal with zero is focused. Fig. 1 shows the overall energy pathway diagram of N_2 electroreduction into NH_3 through dissociative mechanism. The largest barrier for this mechanism is initial $\text{N}\equiv\text{N}$ bond scission to form the adsorbed N atoms with an activation barrier of *ca.* 4.90 eV at -0.22 V (vs. RHE), thus being rate determining step of overall reaction. Although the barrier for N_2 dissociation is significantly decreased at Au(111)/ H_2O electrochemical interface by comparing with that in gas phase (4.90 eV vs. 6.02 eV), it is still extremely high and difficult to be overcome. An activation barrier of *ca.* 1.75 eV is required for initial N_2 electroreduction into N_2H species at the present simulated Au(111)/ H_2O interface in associative mechanisms, as can be seen in Fig. 5. The barrier for N_2H further electroreduction into the surface adsorbed NHNH and NNH_2 species in alternating and distal pathways is calculated as *ca.* 0.22 and 0.01 eV, respectively, suggesting that both NHNH and NNH_2 species are possible key intermediates during N_2 electroreduction on Au(111) because of extremely low formation barriers.

Beginning with NHNH further electroreduction in alternating pathways, we find that the adsorbed NHNH_2 species is unstable at Au(111)/ H_2O interface, which can be spontaneously

electrochemically reduced to form the surface adsorbed NH_2NH_2 species by proton-coupled electron transfer with the surmountable barrier of *ca.* 0.24 eV at room temperature, as shown in Fig. 5(a). The first NH_3 molecule can be produced by further electroreduction of NH_2NH_2 species through two elementary reaction steps including NH_2NH_3 formation and its subsequent N–N bond scission. The corresponding barrier is calculated as *ca.* 0.48 and 0.69 eV, respectively. It is noted that the barrier for NH_2NH_3 further electrodissociation into the adsorbed NH_2 species and NH_3 product is significantly decreased at Au(111)/ H_2O interface compared with that in gas phase (0.69 eV vs. 1.66 eV), suggesting that the presence of electrochemical interface may be able to alter N_2 reduction mechanisms. The formed NH_2 species can finally lead to production of the second NH_3 molecule with an activation barrier of *ca.* 0.56 eV. Starting with NNH_2 intermediate formed in distal pathways, it is found that the adsorbed NHNH_2 and NNH_3 species observed in gas phase are unstable at Au(111)/ H_2O interface, which can be also spontaneously electrochemically reduced to form the surface adsorbed NH_2NH_2 and NHNH_3 intermediates by proton-coupled electron transfer process. The required barrier for NNH_2 electroreduction into NH_2NH_2 and NHNH_3 is calculated as only *ca.* 0.11 and 0.05 eV, respectively, as shown in Fig. 5(b), suggesting that NH_2NH_2 and NHNH_3 species is possible intermediate in distal pathways. Similarly, NH_2NH_2 intermediate can be further electrochemically reduced to form the adsorbed NH_2 species and the first NH_3 molecule *via* abovementioned two elementary reaction steps. Two possibilities are also considered for further electroreduction of NHNH_3 intermediate at Au(111)/ H_2O interface, one is NH_2NH_3 formation, and another is formation of the adsorbed NH species and production of the first NH_3 molecule *via* N–N bond scission. It is found that the required barrier for the former is notably lower than that of the latter (0.24 eV vs. 0.94 eV), indicating that NH_2NH_3 formation is more favorable. Thus, we can concluded that the first NH_3 molecule is possible to be produced by N–N bond scission of NH_2NH_3 species at Au(111)/ H_2O interface, rather than NHNH_3 species as observed in gas phase, again suggesting that the influence of electrochemical interface containing solvation effect on N_2 reduction pathways. The corresponding energetics of for various possible reaction steps involved during

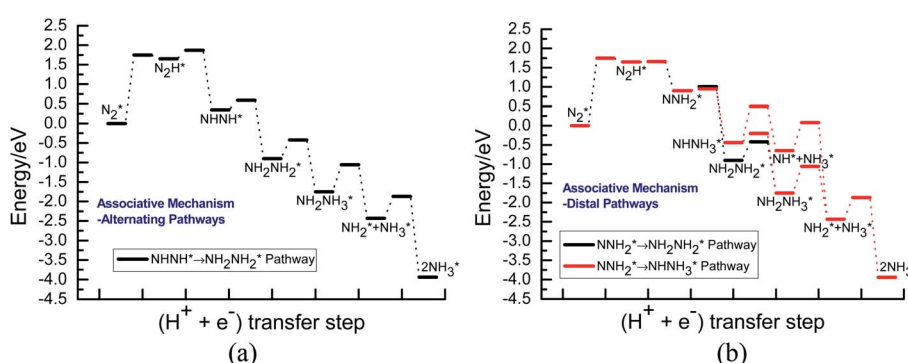


Fig. 5 Overall energy pathway diagram of N_2 electroreduction into NH_3 via associative mechanism at the present proposed Au(111)/ H_2O interface: (a) alternating pathways; (b) distal pathways.



Table 2 Activation barriers (ΔE_{act} , eV) and reaction energies (ΔE_{reac} , eV) for various possible reaction steps involved in N_2 electroreduction pathways at $Au(111)/H_2O$ interface

Reaction steps ^a	ΔE_{act} , eV	ΔE_{reac} , eV
$N_2 + * \rightarrow N^* + N^*$	4.93	4.92
$N^* + (H + e^-) \rightarrow NH^*$	0.33	-1.37
$NH^* + (H + e^-) \rightarrow NH_2^*$	0.73	-1.78
$NH_2^* + (H + e^-) \rightarrow NH_3^*$	0.56	-1.51
$N_2 + * + (H + e^-) \rightarrow N_2H^*$	1.75	1.65
$N_2H^* + (H + e^-) \rightarrow NHNH^*$	0.22	-1.30
$N_2H^* + (H + e^-) \rightarrow NNH_2^*$	0.01	-0.75
$NHNH^* + 2(H + e^-) \rightarrow NH_2NH_2^*$	0.24	-1.25
$NNH_2^* + 2(H + e^-) \rightarrow NH_2NH_2^*$	0.11	-1.80
$NNH_2^* + 2(H + e^-) \rightarrow NHNH_3^*$	0.05	-1.34
$NH_2NH_2^* + (H + e^-) \rightarrow NH_2NH_3^*$	0.48	-0.85
$NHNH_3^* + (H + e^-) \rightarrow NH_2NH_3^*$	0.24	-1.31
$NHNH_3^* \rightarrow NH^* + NH_3^*$	0.94	-0.21
$NH_2NH_3^* \rightarrow NH_2^* + NH_3^*$	0.69	-0.68

^a The asterisk (*) indicates that the species is adsorbed on the $Au(111)$ surface.

N_2 electroreduction at $Au(111)/H_2O$ interface are summarized in Table 2.

By scrutinizing the overall energy pathway diagram, our present simulation results reveal that the rate determining step for N_2 electroreduction into NH_3 via associative alternating and distal mechanisms at $Au(111)/H_2O$ interface is N_2 electroreduction into form the adsorbed N_2H species, suggesting that these both mechanisms may be able to parallelly occur. The corresponding barrier is significantly lower than that of rate determining step in the dissociative mechanism (1.75 eV vs. 4.90 eV). Thus, it can be concluded that the associative mechanisms are more facile to occur at the present simulated $Au(111)/H_2O$ interface. The optimal associative alternating and distal mechanisms are summarized in Fig. 6. Images of

reactants, products and transition states for N_2 electroreduction into NH_3 via the optimal associative mechanisms at the present simulated $Au(111)/H_2O$ interface are included in ESI, as shown in Fig. S14–S23.†

Our present calculated N_2 electroreduction mechanisms at $Au(111)/H_2O$ electrochemical interface are partially inconsistent with the previous theoretical study from Janik *et al.*, in which only alternating pathway via $NHNH$ species is favorable on late transition metals at 0 V (vs. RHE) with rate determining step of N_2 electroreduction into N_2H species by calculating explicitly the potential-dependent barriers for elementary electroreduction reactions (see Fig. 7).⁵¹ Furthermore, the predicted $NHNH_2$ species on late transition metals at 0 V (vs. RHE) is found to be unstable at $Au(111)/H_2O$ interface, which can be spontaneously reduced to form adsorbed NH_2NH_2 species by proton-coupled electron transfer with the surmountable barrier at room temperature. The difference of interface model may lead to partially inconsistent N_2 electroreduction mechanisms, in which only a H_2O molecule is employed to simulate solvent effect in previous theoretical work from Janik *et al.*, being insufficient to model interactions among solvent, adsorbates and surface. However, our present theoretical results can be confirmed by the most recent experimental study from Shao *et al.*, in which the adsorbed intermediates such as N_2H , $NHNH$, NNH_2 , NH_2NH_2 , NH_2NH_3 and NH_2 may be able to be formed during N_2 electroreduction on the Au electrodes at potentials of *ca.* -0.10 V (vs. RHE) or lower due to detected N_2H_y ($1 \leq y \leq 4$) reaction species using the surface-enhanced infrared absorption spectroscopy technique,⁴² further validating the rationality of our present employed $Au(111)/H_2O$ interface model. Simultaneously, we also note that the presence of electrochemical interface makes the barrier of rate determining step in the associative mechanisms decrease compared with that in gas phase (1.75 eV vs. 2.10 eV), indicating that the presence of solvent effect could help stabilize the adsorbed N_2H species and lower the corresponding barrier value to *ca.* 1.75 eV. Even so, barrier of 1.75 eV is still high for N_2 electroreduction, making

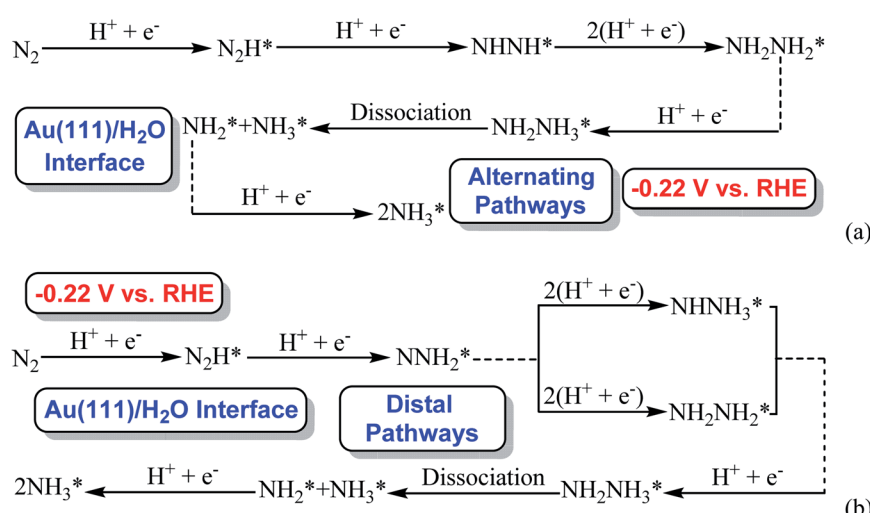


Fig. 6 The optimal associative mechanisms at the present simulated $Au(111)/H_2O$ interface: (a) alternating pathways via $NHNH$ species; (b) distal pathways via NNH_2 species (* represents surface adsorption).



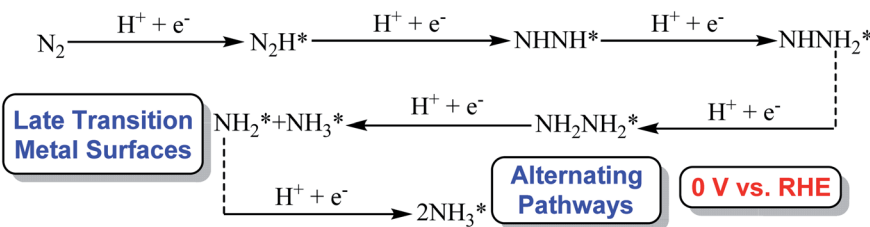


Fig. 7 The optimal associative alternating pathways via NHNH species on late transition metal surfaces at 0 V (vs. RHE) from previous work conducted by Janik *et al.* (* represents surface adsorption).⁵¹

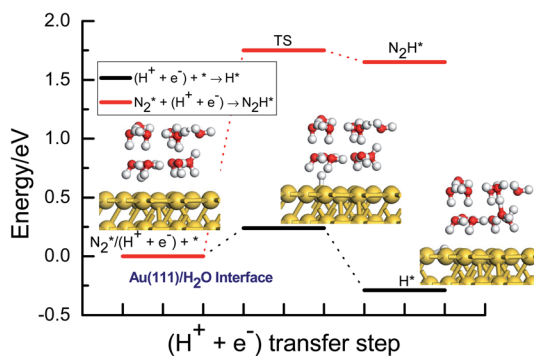


Fig. 8 Energy pathway diagram of competitive hydrogen evolution reaction and initial N₂ electroreduction into N₂H species at the present proposed Au(111)/H₂O electrochemical interface.

this process be still challenging, which may be able to be regarded as origin of experimentally observed high overpotential. The almost not changed N≡N bond length of *ca.* 1.11 Å at Au(111)/H₂O interface again shows weakly adsorbed N₂ molecule compared with that of isolated N₂ molecule.

The potential of the hydrogen evolution reaction is very approximate to the thermodynamically required potential for N₂ electroreduction under ambient conditions. Therefore, overcoming the undesirable hydrogen evolution reaction competition may become the critical challenge during N₂ electroreduction at present, which can greatly reduce the faradaic efficiency of reaction. Herein, the barrier of hydrogen evolution reaction is evaluated by using our present proposed H coverage-dependent Au(111)/H₂O interface model at -0.22 V (vs. RHE) and compared with that of rate determining step for the optimal associative mechanisms during N₂ electroreduction into NH₃ to quantify the challenge in designing the high efficient electrocatalysts. As can be seen in Fig. 8, the calculated activation barrier of *ca.* 0.24 eV is remarkably lower than that of initial N₂ electroreduction into N₂H intermediate (*ca.* 1.75 eV). Furthermore, we also observe that the formed N₂H intermediate may be unstable, which can be facile to back to N₂ molecule with extremely low barrier of *ca.* 0.10 eV. The present comparison and analysis can well explain why the catalytic activity of Au electrodes is usually unsatisfactory although the relatively high faradaic efficiency can be achieved experimentally during N₂ electroreduction.^{24,25,42} Accordingly, the single descriptor may be able to be proposed to scale catalytic activity of electrocatalysts for N₂ electroreduction, in which an ideal

electrocatalyst should be able to reduce barrier for initial N₂ electroreduction into N₂H intermediate. In this way, N₂ electroreduction pathways can be facilitated and the yield of NH₃ can be enhanced.

3.3 Origin of solvation effect on N₂ reduction mechanisms

As above discussed, the presence of electrochemical interface including solvation effect could change N₂ reduction mechanism, especially it can reduce the barrier of rate determining step. To ascertain the origin of difference of N₂ reduction mechanisms at gas phase and the present simulated electrochemical interface on Au(111), the charge density difference analyses are carried out in our present work taking example for N₂ adsorption on Au(111). It is observed that there is almost not significant electron accumulation and interaction between N₂ molecule and surface Au atoms under gas- and aqueous-phase environment, as shown in Fig. 9, confirming the above-mentioned weakly binding N₂ molecule on Au(111) and almost identical N≡N bond length compared with isolated N₂ molecule, thus explaining why high barrier is required for initial N₂ reduction. However, the significant electron interactions are found between N₂ and H₂O cluster at the present simulated electrochemical interface. The existence of H bonds and interactions of N₂ with H₂O molecules at the Au(111)/H₂O interface may lead to easier initial N₂ electroreduction, as observed decreased barrier value.

Based on the above conclusions, we can conclude that the decreased barrier for rate determining step may be able to be ascribed to electronic interactions between N₂ and H₂O cluster. Therefore, the quantitative analysis of electronic structures will facilitate well understanding the origin of solvation effect on N₂ electroreduction mechanisms. According to projected electron densities of states, the Löwdin charge (the number of valence electron) of N₂ can be obtained from Löwdin population analyses on Au(111) in gas phase and at the present simulated electrochemical interface. Table 3 gives the electron gains (Δq) for N₂ molecule, respectively, which could be obtained by subtracting the Löwdin charge of isolated N₂ molecule from that in the optimized structure. Simultaneously, Δq of H₂O cluster at the present simulated electrochemical interfaces are also given in Table 3 compared with that of free N₂ adsorbed Au(111)/H₂O interface. A positive value of Δq will imply a gain of electron by the component. It can be found that only slight electron transfer occurs between N₂ molecule and Au(111) surface in gas phase due to little electron gains of total, s and p orbitals of N₂, as



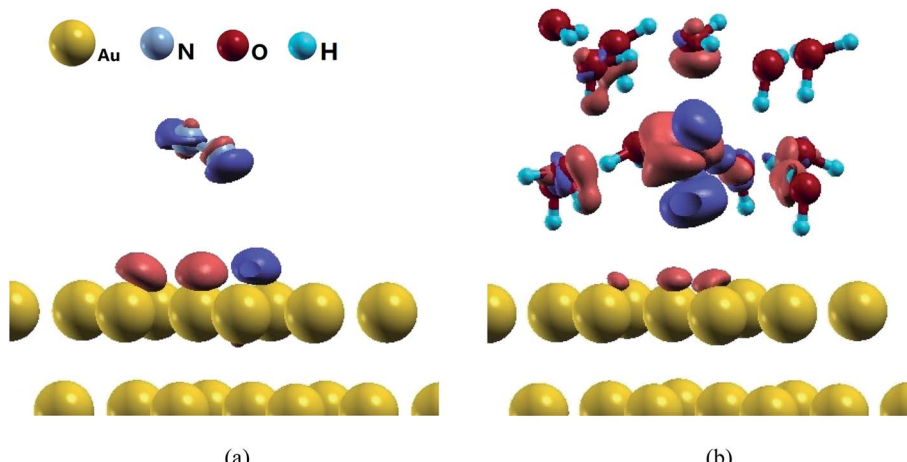


Fig. 9 The charge density difference maps for N_2 (a) in gas-phase and (b) at the Au(111)/ H_2O interface.

Table 3 The electron gains (Δq) of total, s and p orbitals of N_2 molecule on Au(111) and at the present simulated Au(111)/ H_2O interface; Δq of total, s and p orbitals of H_2O cluster in N_2 adsorbed Au(111)/ H_2O interface

		Difference of electron (Δq)		
		Total	s	p
Au(111)	N_2	-0.0284	-0.0271	-0.0013
Au(111)/ H_2O interface	N_2	-0.0147	-0.0385	+0.0238
	H_2O cluster	+0.0188	+0.0384	-0.0195

found weakly bonded N_2 molecule on Au(111) with the adsorption energy of only *ca.* -0.03 eV, confirming the above observed no significant electron accumulation and interaction based on the charge density difference analyses. However, we notice that the nature of electronic interactions at the Au(111)/ H_2O interface is practically not the same as that observed in gas phase. The significant electron transfer occurs between N_2 molecule and H_2O cluster, namely, the total net electrons of H_2O cluster are positive because s orbital can gain more electrons although p orbital loses electrons, whereas the total net electrons of N_2 is negative, in which s orbital loses electrons and p orbital gains electrons. Thus, it can be concluded that the notable different electron interactions on Au(111) in gas phase and at the electrochemical interface may result in the difference of N_2 reduction mechanisms.

4. Conclusions

In the present paper, an improved H coverage-dependent Au(111)/ H_2O electrochemical interface model is proposed, which is firstly used to study electroreduction mechanisms of N_2 to NH_3 at the thermodynamical equilibrium potential cooperated with electronic structure analysis. The calculated results show that the associative mechanism is more favorable on Au(111) and therein alternating and distal pathways may be

able to parallelly occur in gas phase and the present simulated electrochemical interface. The initial N_2 reduction into N_2H intermediate is rate determining step, which may be able to be regarded as the origin of observed experimentally high overpotential during N_2 electroreduction. However, the presence of electrochemical environment can significantly change N_2 reduction pathway and decrease the barrier of rate determining step, in which NHNH_2 and NNH_3 species observed in gas phase are unstable at Au(111)/ H_2O interface, which can be spontaneously electrochemically reduced to form adsorbed NH_2NH_2 and NHNH_3 intermediates by proton-coupled electron transfer process. The significant electron accumulation and interaction between N_2 molecule and H_2O cluster may result in different N_2 electroreduction pathways and the decreased barrier of rate determining step. The theoretical results display excellent consistency with the available experimental data, confirming the rationality of the present used Au(111)/ H_2O interface model. The comparison of barrier between hydrogen evolution reaction and rate determining step well explains why the catalytic activity of Au electrodes is usually unsatisfactory although the relatively high faradaic efficiency can be experimentally achieved. Accordingly, the single descriptor may be able to be proposed, in which an ideal electrocatalyst should be able to reduce barrier for initial N_2 electroreduction into N_2H intermediate. In this way, N_2 electroreduction pathways can be facilitated and the yield of NH_3 can be enhanced. We believe that the present study represents a progress to systematically study N_2 electroreduction mechanisms based on an improved electrochemical interface model.

Conflicts of interest

There are no conflicts to declare.

Acknowledgements

This work was supported by the Key Program of Education Department of Hunan Province (Grant No. 19A337); Hunan Provincial Natural Science Foundation of China (Grant No.



2018JJ2273); Key Program of Hunan University of Arts and Science (19ZD06) and National Natural Science Foundation of China (Grant No. 21303048).

References

- 1 V. Smil, Detonator of the Population Explosion, *Nature*, 1999, **400**, 415.
- 2 J. G. Chen, R. M. Crooks, L. C. Seefeldt, K. L. Bren, R. M. Bullock, M. Y. Daresbourg, P. L. Holland, B. Hoffman, M. J. Janik, A. K. Jones, M. G. Kanatzidis, P. King, K. M. Lancaster, S. V. Lymar, P. Pfromm, W. F. Schneider and R. R. Schrock, Beyond Fossil Fuel-Driven Nitrogen Transformations, *Science*, 2018, **360**, eaar6611.
- 3 A. Klerke, C. H. Christensen, J. K. Nørskov and T. Vegge, Ammonia for Hydrogen Storage: Challenges and Opportunities, *J. Mater. Chem.*, 2008, **18**, 2304–2310.
- 4 J. A. Pool, E. Lobkovsky and P. J. Chirik, Hydrogenation and Cleavage of Dinitrogen to Ammonia with a Zirconium Complex, *Nature*, 2004, **427**, 527–530.
- 5 G. Ertl, Reactions at Surfaces: From Atoms to Complexity, *Angew. Chem., Int. Ed.*, 2008, **47**, 3524–3535.
- 6 H. K. Lee, C. S. L. Koh, Y. H. Lee, C. Liu, I. Y. Phang, X. Han, C. K. Tsung and X. Y. Ling, Favoring the Unfavored: Selective Electrochemical Nitrogen Fixation Using a Reticular Chemistry Approach, *Sci. Adv.*, 2018, **4**, eaar3208.
- 7 M. Kitano, Y. Inoue, Y. Yamazaki, F. Hayashi, S. Kanbara, S. Matsuishi, T. Yokoyama, S. W. Kim, M. Hara and H. Hosono, Ammonia Synthesis Using a Stable Electride as an Electron Donor and Reversible Hydrogen Store, *Nat. Chem.*, 2012, **4**, 934–940.
- 8 J. W. Erisman, M. A. Sutton, J. Galloway, Z. Klimont and W. Winiwarter, How a Century of Ammonia Synthesis Changed the World, *Nat. Geosci.*, 2008, **1**, 636–639.
- 9 C. J. M. van der Ham, M. T. M. Koper and D. G. H. Hetterscheid, Challenges in Reduction of Dinitrogen by Proton and Electron Transfer, *Chem. Soc. Rev.*, 2014, **43**, 5183–5191.
- 10 V. Kyriakou, I. Garagounis, E. Vasileiou, A. Vourros and M. Stoukides, Progress in the Electrochemical Synthesis of Ammonia, *Catal. Today*, 2017, **286**, 2–13.
- 11 M. A. Shipman and M. Symes, Recent Progress towards the Electrosynthesis of Ammonia from Sustainable Resources, *Catal. Today*, 2017, **286**, 57–68.
- 12 C. X. Guo, J. R. Ran, A. Vasileff and S. Z. Qiao, Rational Design of Electrocatalysts and Photo (Electro) Catalysts for Nitrogen Reduction to Ammonia (NH_3) under Ambient Conditions, *Energy Environ. Sci.*, 2018, **11**, 45–56.
- 13 N. Cao and G. F. Zheng, Aqueous Electrocatalytic N_2 Reduction under Ambient Conditions, *Nano Res.*, 2018, **11**, 2992–3008.
- 14 J. Deng, J. A. Iñiguez and C. Liu, Electrocatalytic Nitrogen Reduction at Low Temperature, *Joule*, 2018, **2**, 846–856.
- 15 J. H. Montoya, C. Tsai, A. Vojvodic and J. K. Nørskov, The Challenge of Electrochemical Ammonia Synthesis: A New Perspective on the Role of Nitrogen Scaling Relations, *ChemSusChem*, 2015, **8**, 2180–2186.
- 16 R. Ran, J. T. S. Irvine and S. Tao, Synthesis of Ammonia Directly from Air and Water at Ambient Temperature and Pressure, *Sci. Rep.*, 2013, **3**, 1145.
- 17 S. Licht, B. Cui, B. Wang, F. F. Li, J. Lau and S. Liu, Ammonia Synthesis by N_2 and Steam Electrolysis in Molten Hydroxide Suspensions of Nanoscale Fe_2O_3 , *Science*, 2014, **345**, 637–640.
- 18 G. Qing, R. Kikuchi, S. Kishira, A. Takagaki, T. Sugawara and S. T. Oyama, Ammonia Synthesis by N_2 and Steam Electrolysis in Solid-State Cells at 220 °C and Atmospheric Pressure, *J. Electrochem. Soc.*, 2016, **163**, E282–E287.
- 19 V. Kordali, G. Kyriacou and C. Lambrou, Electrochemical Synthesis of Ammonia at Atmospheric Pressure and Low Temperature in a Solid Polymer Electrolyte Cell, *Chem. Commun.*, 2000, **17**, 1673–1674.
- 20 Y. Yao, H. J. Wang, X. Z. Yuan, H. Li and M. H. Shao, Electrochemical Nitrogen Reduction on Ruthenium, *ACS Energy Lett.*, 2019, **4**, 1336–1341.
- 21 K. Imamura and J. Kubota, Electrochemical Membrane Cell for NH_3 Synthesis from N_2 and H_2O by Electrolysis at 200 to 250 °C Using a Ru Catalyst, Hydrogen-Permeable Pd Membrane and Phosphate-Based Electrolyte, *Sustain. Energy Fuels*, 2018, **2**, 1278–1286.
- 22 K. Kugler, M. Luhn, J. A. Schramm, K. Rahimi and M. Wessling, Galvanic Deposition of Rh and Ru on Randomly Structured Ti Felts for the Electrochemical NH_3 Synthesis, *Phys. Chem. Chem. Phys.*, 2015, **17**, 3768–3782.
- 23 J. Wang, L. Yu, L. Hu, G. Chen, H. L. Xin and X. F. Feng, Ambient Ammonia Synthesis via Palladium-Catalyzed Electrohydrogenation of Dinitrogen at Low Overpotential, *Nat. Commun.*, 2018, **9**, 1795.
- 24 S. J. Li, D. Bao, M. M. Shi, B. R. Wulan, J. M. Yan and Q. Jiang, Amorphizing of Au Nanoparticles by CeO_x -RGO Hybrid Support towards Highly Efficient Electrocatalyst for N_2 Reduction under Ambient Conditions, *Adv. Mater.*, 2017, **29**, 1700001.
- 25 M. M. Shi, D. Bao, B. R. Wulan, Y. H. Li, Y. F. Zhang, J. M. Yan and Q. Jiang, Au Sub-Nanoclusters on TiO_2 toward Highly Efficient and Selective Electrocatalyst for N_2 Conversion to NH_3 at Ambient Conditions, *Adv. Mater.*, 2017, **29**, 1606550.
- 26 H. M. Liu, S. H. Han, Y. Zhao, Y. Y. Zhu, X. L. Tian, J. H. Zeng, J. X. Jiang, B. Y. Xia and Y. Chen, Surfactant-Free Atomically Ultrathin Rhodium Nanosheet Nanoassemblies for Efficient Nitrogen Electroreduction, *J. Mater. Chem. A*, 2018, **6**, 3211–3217.
- 27 X. R. Zhao, F. X. Yin, N. Liu, G. R. Li, T. X. Fan and B. H. Chen, Highly Efficient Metal-Organic-Framework Catalysts for Electrochemical Synthesis of Ammonia from N_2 (Air) and Water at Low Temperature and Ambient Pressure, *J. Mater. Sci.*, 2017, **52**, 10175–10185.
- 28 K. Kim, C. Y. Yoo, J. N. Kim, H. C. Yoon and J. I. Han, Electrochemical Synthesis of Ammonia from Water and Nitrogen in Ethylenediamine under Ambient Temperature and Pressure, *J. Electrochem. Soc.*, 2016, **163**, F1523–F1526.
- 29 D. S. Yang, T. Chen and Z. J. Wang, Electrochemical Reduction of Aqueous Nitrogen (N_2) at a Low Overpotential



on (110)-Oriented Mo Nanofilm, *J. Mater. Chem. A*, 2017, **5**, 18967–18971.

30 Y. C. Hao, Y. Guo, L. W. Chen, M. Shu, X. Y. Wang, T. A. Bu, W. Y. Gao, N. Zhang, X. Su, X. Feng, J. W. Zhou, B. Wang, C. W. Hu, A. X. Yin, R. Si, Y. W. Zhang and C. H. Yan, Promoting Nitrogen Electroreduction to Ammonia with Bismuth Nanocrystals and Potassium Cations in Water, *Nat. Catal.*, 2019, **2**, 448–456.

31 R. Manjunatha and A. Schechter, Electrochemical Synthesis of Ammonia Using Ruthenium-Platinum Alloy at Ambient Pressure and Low Temperature, *Electrochem. Commun.*, 2018, **90**, 96–100.

32 L. Zhang, X. Q. Ji, X. Ren, Y. J. Ma, X. F. Shi, Z. Q. Tian, A. M. Asiri, L. Chen, B. Tang and X. P. Sun, Electrochemical Ammonia Synthesis via Nitrogen Reduction Reaction on a MoS₂ Catalyst: Theoretical and Experimental Studies, *Adv. Mater.*, 2018, **30**, 1800191.

33 X. P. Zhang, R. M. Kong, H. T. Du, L. Xia and F. L. Qu, Highly Efficient Electrochemical Ammonia Synthesis via Nitrogen Reduction Reactions on a VN Nanowire Array under Ambient Conditions, *Chem. Commun.*, 2018, **54**, 5323–5325.

34 S. M. Chen, S. Perathoner, C. Ampelli, C. Mebrahtu, D. S. Su and G. Centi, Electrocatalytic Synthesis of Ammonia at Room Temperature and Atmospheric Pressure from Water and Nitrogen on a Carbon nanotube-Based electrocatalyst, *Angew. Chem., Int. Ed.*, 2017, **56**, 2699–2703.

35 Y. M. Liu, Y. Su, X. Quan, X. F. Fan, S. Chen, H. T. Yu, H. M. Zhao, Y. B. Zhang and J. J. Zhao, Facile Ammonia Synthesis from Electrocatalytic N₂ Reduction under Ambient Conditions on N-Doped Porous Carbon, *ACS Catal.*, 2018, **8**, 1186–1191.

36 C. Lv, Y. Qian, C. Yan, Y. Ding, Y. Liu, G. Chen and G. Yu, Defect Engineering Metal-Free Polymeric Carbon Nitride Electrocatalyst for Effective Nitrogen Fixation under Ambient Conditions, *Angew. Chem., Int. Ed.*, 2018, **57**, 10246–10250.

37 Y. Abghoui and E. Skulason, Computational Predictions of Catalytic Activity of Zincblende (110) Surfaces of Metal Nitrides for Electrochemical Ammonia Synthesis, *J. Phys. Chem. C*, 2017, **121**, 6141–6151.

38 S. Mukherjee, D. A. Cullen, S. Karakalos, K. X. Liu, H. Zhang, S. Zhao, H. Xu, K. L. More, G. F. Wang and G. Wu, Metal-Organic Framework-Derived Nitrogen-Doped Highly Disordered Carbon for Electrochemical Ammonia Synthesis Using N₂ and H₂O in Alkaline Electrolytes, *Nano Energy*, 2018, **48**, 217–226.

39 Y. Yao, J. Wang, U. B. Shahid, M. Gu, H. J. Wang, H. Li and M. H. Shao, Electrochemical Synthesis of Ammonia from Nitrogen Under Mild Conditions: Current Status and Challenges, *Electrochem. Energy Rev.*, 2020, **3**, 239–270.

40 R. Manjunatha, A. Karajic, M. Liu, Z. B. Zhai, L. Dong, W. Yan, D. P. Wilkinson and J. J. Zhang, A Review of Composite/Hybrid Electrocatalysts and Photocatalysts for Nitrogen Reduction Reactions: Advanced Materials, Mechanisms, Challenges and Perspectives, *Electrochem. Energy Rev.*, 2020, **3**, 506–540.

41 G. Ertl, Surface Science and Catalysis-Studies on the Mechanism of Ammonia Synthesis: The P. H. Emmett Award Address, *Catal. Rev.*, 1980, **21**, 201–223.

42 Y. Yao, S. Q. Zhu, H. J. Wang, H. Li and M. H. Shao, A Spectroscopic Study on the Nitrogen Electrochemical Reduction Reaction on Gold and Platinum Surfaces, *J. Am. Chem. Soc.*, 2018, **140**, 1496–1501.

43 J. K. Nørskov, T. Bligaard, J. Rossmeisl and C. H. Christensen, Towards the Computational Design of Solid Catalysis, *Nat. Chem.*, 2009, **1**, 37–46.

44 J. K. Nørskov, F. Abild-Pedersen, F. Studt and T. Bligaard, Density Functional Theory in Surface Chemistry and Catalysis, *Proc. Natl. Acad. Sci. U. S. A.*, 2011, **108**, 937–943.

45 E. Skúlason, T. Bligaard, S. Gudmundsdóttir, F. Studt, J. Rossmeisl, F. Abild-Pederson, T. Vegge, H. Jósson and J. K. Nørskov, A Theoretical Evaluation of Possible Transition Metal Electro-Catalysts for N₂ Reduction, *Phys. Chem. Chem. Phys.*, 2012, **14**, 1235–1245.

46 H. Y. Li, Z. F. Zhao, Q. H. Cai, L. C. Yin and J. X. Zhao, Nitrogen Electroreduction Performance of Transition Metal Dimers Embedded into N-Doped Graphene: A Theoretical Prediction, *J. Mater. Chem. A*, 2020, **8**, 4533–4543.

47 G. Rostamikia, A. J. Mendoza, M. A. Hickner and M. J. Janik, First-Principles Based Microkinetic Modeling of Borohydride Oxidation on a Au(111) Electrode, *J. Power Sources*, 2011, **196**, 9228–9237.

48 X. W. Nie, M. R. Esopi, M. J. Janik and A. Asthagiri, Selectivity of CO₂ Reduction on Copper Electrodes: The Role of the Kinetics of Elementary Steps, *Angew. Chem., Int. Ed.*, 2013, **52**, 2459–2462.

49 S. A. Akhade, N. J. Bernstein, M. R. Esopi, M. J. Regula and M. J. Janik, Electrochemical Reduction of Carbon Dioxide by Heterogenous and Homogeneous Catalysts: Experiment and Theory, *Catal. Today*, 2017, **288**, 63–73.

50 S. Maheshwari, G. Rostamikia and M. J. Janik, Elementary Kinetics of Nitrogen Electroreduction on Fe Surfaces, *J. Chem. Phys.*, 2019, **150**, 041708.

51 G. Rostamikia, S. Maheshwari and M. J. Janik, Elementary Kinetics of Nitrogen Electroreduction to Ammonia on Late Transition Metals, *Catal. Sci. Technol.*, 2019, **9**, 174–181.

52 D. Bao, Q. Zhang, F. L. Meng, H. X. Zhong, M. M. Shi, Y. Zhang, J. M. Yang, Q. Jiang and X. B. Zhang, Electrochemical Reduction of N₂ under Ambient Conditions for Artificial N₂ Fixation and Renewable Energy Storage Using N₂/NH₃ Cycle, *Adv. Mater.*, 2017, **29**, 1604799.

53 L. H. Ou, J. X. Chen, Y. D. Chen and J. L. Jin, Mechanistic Study of Pt-Catalyzed Electrooxidation of HCOOH in Acid Medium: Kinetic Considerations on the Effect of Solvation, *J. Phys. Chem. C*, 2018, **122**, 24871–24884.

54 L. H. Ou, Theoretical Insights into the Effect of Solvation and Sublayer Ru on Pt-Catalytic CH₃OH Oxidation Mechanisms in the Aqueous Phase, *J. Phys. Chem. C*, 2018, **122**, 14554–14565.

55 L. H. Ou, J. X. Chen, Y. D. Chen and J. L. Jin, Mechanistic Study on Cu-catalyzed CO₂ Electrocatalysis into CH₄ at Simulated Low Overpotentials Based on an Improved



Electrochemical Model, *Phys. Chem. Chem. Phys.*, 2019, **21**, 15531–15540.

56 E. Skúlason, V. Tripkovic, M. E. Björketun, S. Gudmundsdóttir, G. Karlberg, J. Rossmeisl, T. Bligaard, H. Jónsson and J. K. Nørskov, Modeling the Electrochemical Hydrogen Oxidation and Evolution Reactions on the Basis of Density Functional Theory Calculations, *J. Phys. Chem. C*, 2010, **114**, 18182–18197.

57 E. Skúlason, G. S. Karlberg, J. Rossmeisl, T. Bligaard, J. Greeley, H. Jónsson and J. K. Nørskov, Density Functional Theory Calculations for the Hydrogen Evolution Reaction in an Electrochemical Double Layer on the Pt(111) Electrode, *Phys. Chem. Chem. Phys.*, 2007, **9**, 3241–3250.

58 J. Rossmeisl, E. Skúlason, M. E. Björketun, V. Tripkovic and J. K. Nørskov, Modeling the Electrified Solid-Liquid Interface, *Chem. Phys. Lett.*, 2008, **466**, 68–71.

59 J. K. Nørskov, J. Rossmeisl, A. Logadóttir, L. Lindqvist, J. R. Kitchin, T. Bligaard and H. Jónsson, Origin of the Overpotential for Oxygen Reduction at a Fuel-Cell Cathode, *J. Phys. Chem. B*, 2004, **108**, 17886–17892.

60 G. S. Karlberg, T. F. Jaramillo, E. Skúlason, J. Rossmeisl, T. Bligaard and J. K. Nørskov, Cyclic Voltammograms for H on Pt(111) and Pt(100) from First Principles, *Phys. Rev. Lett.*, 2007, **99**, 126101.

61 J. K. Nørskov, T. Bligaard, A. Logadóttir, J. R. Kitchin, J. G. Chen, S. Pandelov and U. Stimming, Trends in the Exchange Current for Hydrogen Evolution, *J. Electrochem. Soc.*, 2005, **152**, J23–J26.

62 F. Yang, Q. F. Zhang, Y. W. Liu and S. L. Chen, A Theoretical Consideration on the Surface Structure and Nanoparticle Size Effects of Pt in Hydrogen Electrocatalysis, *J. Phys. Chem. C*, 2011, **115**, 19311–19319.

63 H. Mistry, R. Reske, Z. H. Zeng, Z. J. Zhao, J. Greeley, P. Strasser and B. R. Cuenya, Exceptional Size-Dependent Activity Enhancement in the Electroreduction of CO₂ over Au Nanoparticles, *J. Am. Chem. Soc.*, 2014, **136**, 16473–16476.

64 A. A. Peterson, F. Abild-Pederson, F. Studt, J. Rossmeisl and J. K. Nørskov, How Copper Catalyzes the Electrodissolution of Carbon Dioxide into Hydrocarbon Fuels, *Energy Environ. Sci.*, 2010, **3**, 1311–1315.

